

# Light-Induced Intramolecular Electron Transfer in a 1D [CuFe] Coordination Polymer Containing the $[\text{Fe}(\text{C}_2\text{O}_4)_3]^{3-}$ Core

*Lidija Molčanov,<sup>a</sup> Lidija Androš Dubraja,<sup>a</sup> Dijana Žilić,<sup>a</sup> Krešimir Molčanov,<sup>a</sup>  
Dario Barišić,<sup>b</sup> Damir Pajić,<sup>b</sup> Ivor Lončarić,<sup>a</sup> Ana Šantić<sup>a</sup> and Marijana Jurić<sup>a,\*</sup>*

<sup>a</sup>Ruđer Bošković Institute, Bijenička cesta 54, 10000 Zagreb, Croatia

<sup>b</sup>Department of Physics, Faculty of Science, University of Zagreb, Bijenička cesta 54,

10000 Zagreb, Croatia

**ABSTRACT.** A one-dimensional (1D) ladder-like coordination polymer  $\{\text{NH}_4[\{\text{Cu}(\text{bpy})\}_2(\text{C}_2\text{O}_4)\text{Fe}(\text{C}_2\text{O}_4)_3]\cdot\text{H}_2\text{O}\}_n$  (**1**; bpy = 2,2'-bipyridine) containing  $[\text{Cu}(\text{bpy})(\mu\text{-C}_2\text{O}_4)\text{Cu}(\text{bpy})]^{2+}$  cationic units linked by oxalate groups of  $[\text{Fe}(\text{C}_2\text{O}_4)_3]^{3-}$  building blocks was investigated as a new type of photoactive solid-state system. It exhibits a photocoloration effect when exposed to direct sunlight or UV/Vis irradiation. The photochromic properties and mechanism were studied by powder and single-crystal X-ray diffraction, UV/Vis diffuse reflectance, IR and EPR spectroscopy, magnetization and impedance measurements, and DFT calculations. The process of photochromism involves simultaneous intramolecular electron transfers from the oxalate ligand to Fe(III) and to  $[\text{Cu}^{\text{II}}(\text{bpy})(\mu\text{-C}_2\text{O}_4)\text{Cu}^{\text{II}}(\text{bpy})]^{2+}$ , leading to the reduction of the metal centres to the electronic states Fe(II) and Cu(I), accompanied by the release of gaseous  $\text{CO}_2$ .

## INTRODUCTION

Stimulative and switchable materials exhibit two or more stable, observable or detectable properties in response to external stimuli (as light, temperature, solvent molecules, pressure, pH, electric or magnetic field variations) at the micro- or nanoscale and have recently attracted more interest due to the possible uses in numerous fields. In general, chemical, physical, and biochemical inputs are the three main categories of stimuli. Ionic solvents, pH, chemical agents, or electrolytes are examples of chemical stimuli; physical stimuli such as temperature, light, mechanical force, electric and magnetic fields are widely used, while biochemical stimuli include enzymes, antigens, ligands and biochemical agents.<sup>1-6</sup>

Photochromic materials can display reversible changes in their molecular and electrical structure when exposed to light. The absorption of electromagnetic radiation causes the reversible change of a chemical species between two forms, A and B, with differing absorption spectra. Irradiation converts the thermodynamically stable form A to the less stable form B, which has different absorption spectra and can be restored to form A either thermally or photochemically. Interconversion of two states is typically accompanied by a change in physical properties such as structural transformation, dielectric constant, electric conductivity, magnetism, luminescence, mechanical effect, refractive index, redox potential, solubility, viscosity, or surface wettability.<sup>7-9</sup>

Metal-organic coordination polymers have been highlighted as an acceptable class of switchable materials because to their unique characteristics, excellent component and structure modulation ability due to the variety of inorganic nodes and flexibility of organic linkers. These materials are appealing because they enable easy visual monitoring of changes in certain properties and so have potential uses in domains such as optical switches,

solar energy conversion, data storage, and photomasks. There are several methods for developing metal-organic compounds. The most frequent way is to use a photochromic linker, which can be structurally changed upon exposure to light. Bipyridinium carboxylate linkers, on the other hand, can be employed to build photochromic systems since they can create viologen radicals when irradiated with light. In order to create photochromic metal-organic coordination polymers without photochromic organic linkers, photoinduced bistable systems based on various electron-transfer mechanisms can be used: metal-centered electron transition (MC), ligand-to-metal charge transfer (LMCT), metal-to-metal CT (MMCT), intraligand CT (ILCT), and ligand-to-ligand CT (LLCT). Photochromic metal-organic compounds with electron transfer are electronically labile and have two or more electronic states that are energetically near to one another, resulting in strong vibronic interactions and sensitivity to external photo perturbations. The photoresponsive process depends on many factors such as the ability of electron-donors/acceptors to donate/accept electrons, the nature of packing, and weak interactions. For this reason, rational matching between units of electron donors and acceptors suitable for photoinduced electron transfer and subsequent radical generation is a very challenging task.<sup>6,10-14</sup>

One of the photoresponsive processes in metal-organic systems involves a LMCT reaction, in which an electron is transferred from the ligand to the metal centre, resulting in the formation of a radical ligand. The tris(oxalato)ferrate(III) is a prototype example of such a complex, whose photoinduced LMCT reaction results in the (photo) production of Fe(II) ions (both in solution and in solid state) and a subsequent reductive reaction *via*  $\text{CO}_2^{\bullet-}$  radical anions.<sup>15-19</sup> From the applicative point of view photoreactive complexes

sensitive to visible (Vis) and ultraviolet (UV) light could be of interest in environmental chemistry and photochemical laboratory applications in general (e.g. actinometry).<sup>20</sup>

In this context, we have investigated previously prepared and structurally characterized compound  $\{\text{NH}_4[\{\text{Cu}(\text{bpy})\}_2(\text{C}_2\text{O}_4)\text{Fe}(\text{C}_2\text{O}_4)_3]\cdot\text{H}_2\text{O}\}_n$  (**1**; bpy = 2,2'-bipyridine) as a new sort of solid-state photoactive system, containing  $[\text{Cu}^{\text{II}}(\text{bpy})(\mu\text{-C}_2\text{O}_4)\text{Cu}^{\text{II}}(\text{bpy})]^{2+}$  cationic species units linked by oxalate groups of  $[\text{Fe}^{\text{III}}(\text{C}_2\text{O}_4)_3]^{3-}$  in a ladder-like one-dimensional (1D) coordination polymer. Crystallization of this  $[\text{Cu}^{\text{II}}\text{Fe}^{\text{III}}]$  compound from solution occurs when the test tube containing the reaction mixture is in the dark, i.e., without the presence of light. When the same reaction mixture was exposed to daylight in the test tube, the initial building block  $[\text{Fe}(\text{C}_2\text{O}_4)_3]^{3-}$  in solution endures photoreduction; iron(III) is reduced to the divalent state, resulting in the formation of a three-dimensional (3D)  $\{[\text{Fe}^{\text{II}}_2(\text{C}_2\text{O}_4)_3]\}_n^{2n-}$  network that subsequently leads to crystallization of the reddish  $[\text{Cu}^{\text{II}}\text{Fe}^{\text{II}}]$  coordination polymer  $\{[\text{Cu}(\text{bpy})_3][\text{Fe}_2(\text{C}_2\text{O}_4)_3]\cdot\text{H}_2\text{O}\}_n$ .<sup>21</sup> When exposed to direct sunshine or UV/Vis irradiation in the solid state, the isolated, crystalline product of **1** exhibits substantial photocoloration. Powder and single-crystal X-ray diffraction, UV/Vis diffuse reflectance, IR and EPR spectroscopy, magnetization measurements, impedance spectroscopy, and DFT calculations were used to analyze this apparent effect. We have shown that the process of photocoloration involves simultaneous intramolecular electron transfers from the oxalate ligand to Fe(III) and to  $[\text{Cu}^{\text{II}}(\text{bpy})(\mu\text{-C}_2\text{O}_4)\text{Cu}^{\text{II}}(\text{bpy})]^{2+}$ , leading to reduction of the metal centres to Fe(II) and Cu(I) electronic states, accompanied by the release of gaseous  $\text{CO}_2$ .<sup>15</sup>

## EXPERIMENTAL SECTION

**Materials and Methods.** All chemicals were purchased from commercial sources and used without further purification. The preparation method used for the synthesis of the

ammonium salt of the tris(oxalato)ferrate(III),  $(\text{NH}_4)_3[\text{Fe}(\text{C}_2\text{O}_4)_3]\cdot 3\text{H}_2\text{O}$ , was derived from that of the potassium salt by replacing the potassium reactants with the ammonium homologues.<sup>22</sup> The investigated compound  $\{\text{NH}_4[\{\text{Cu}(\text{bpy})\}_2(\text{C}_2\text{O}_4)\text{Fe}(\text{C}_2\text{O}_4)_3]\cdot \text{H}_2\text{O}\}_n$  (**1**) was prepared according to the procedure described in the literature.<sup>21</sup> Solid-state UV/Vis spectra were obtained at 20 °C using a Shimadzu UV-Vis-NIR spectrometer (model UV-3600) equipped with an integrating sphere. Barium sulphate was used as a reference. First, the initial sample was placed in the sample holder and measured, and then it was irradiated with a Xenon lamp (300 W) for 15 minutes and measured again. The infrared spectra were recorded in the 4000–350  $\text{cm}^{-1}$  region with samples as KBr pellets, with a Bruker Alpha-T spectrometer.

**Preparation of Irradiated Samples of Compound 1.** The blue-green crystals or powder of compound **1** change colour to dark green (**1-irrad**) after irradiation under UV/Vis light. Irradiation was performed using an Asahi Spectra 300 W Xenon Light Source, model MAX-303, equipped with a UV-Vis mirror module (300–600 nm), a 422 nm long-pass filter and a light guide. The sample was placed 10 cm below the light source. After standing in the dark for 14 days, the sample **1-irrad** slowly changes colour back to greenish (**1-recov**). The effect of daylight on compound **1** was also studied (**1-irradD versus 1-recovD**). The powder sample was left to stand on the bench for 5 days under laboratory conditions, during which it gradually turned dark green. For the IR measurements, the sample was irradiated with ten Luzchem LZC-UVA lamps ( $I_{\text{exc}} = 351$  nm; P = 16 W).

**Single-Crystal X-Ray Diffraction.** Single-crystal measurements were performed on a Rigaku Oxford Diffraction Synergy S diffractometer with a HyPix hybrid pixel counting detector, using microfocus CuK $\alpha$  radiation.

**Powder X-Ray Diffraction.** The powder X-ray diffraction (PXRD) data at room temperature for samples **1** and **1-irrad** were collected in reflection mode with Cu K $\alpha$  radiation on a Malvern Panalytical Empyrean diffractometer using a step size of 0.001° in the 2 $\theta$  range between 5° and 50°.

**EPR Study.** Electron paramagnetic resonance (EPR) measurements were performed on powdered samples by an X-band EPR spectrometer (Bruker Elexsys 580 FT/CW) that was equipped with a standard Oxford Instruments model DTC2 temperature controller. The experiments were performed, using liquid nitrogen, in a temperature range 80–295 K. The microwave frequency was around 9.7 GHz, the magnetic field modulation amplitude was 0.5 mT and the modulation frequency was 100 kHz.

**Magnetization Measurements.** The static magnetization of **1** and **1-irrad** in the powder form was measured using a superconducting quantum interference device (SQUID) magnetometer. Measurements were performed at 300 K and field dependence of magnetization M(H) was measured several times to check reproducibility. Susceptibilities and effective magnetic moments were determined as the slopes of the linear M(H) dependences after correction for the contribution of the gelatine ampoule.

**Electrical Study.** The electrical conductivity of **1** and **1-irrad** was measured using impedance spectroscopy (Novocontrol Alpha-N dielectric analyzer) at 20 °C in the range of frequency from 0.01 Hz to 1 MHz. For the measurements, polycrystalline powder was pressed into a disc and gold electrodes (3.8 mm in diameter) were sputtered on its opposite surfaces using a sputter

coater SC7620 (Quorum Technologies). The disc with the gold electrodes was then placed between two gold plated electrodes of the sample cell (Standard sample cell BDS1200, Novocontrol Technologies). The temperature was controlled to an accuracy of  $\pm 0.2$  °C using the Novocool cryosystem (Novocontrol Technologies). The impedance spectra of **1** and **1-irrad** were analysed by equivalent circuit modelling using the complex nonlinear least-squares fitting procedure (ZView software).

**DFT Calculations.** The density functional theory (DFT) calculations were performed using the Quantum ESPRESSO code v6.8.,<sup>23,24</sup> and the plane wave cutoff of 108 Ry was used. The Brillouin zone was sampled with k-points of the density of at least 4 Å, using the so-called SSSP Efficiency pseudopotentials.<sup>25</sup> The PBE exchange-correlation functional<sup>26</sup> with +U correction<sup>27</sup> of 6 eV for Cu d orbitals and 2 eV for Fe d orbitals was used. The structure was relaxed until default criteria were met, i.e. the change in energy was less than 0.0001 Ry, and forces on all atoms were smaller than 0.001 Ry/a0. The unit cell was fixed to the experimental value.

## RESULTS AND DISCUSSION

**Crystal Structure of Compound 1 and Preparation of the Irradiated Compound 1.** In this work, we have investigated the photoresponsive properties of a previously reported 1D coordination polymer  $\{\text{NH}_4[\{\text{Cu}(\text{bpy})\}_2(\text{C}_2\text{O}_4)\text{Fe}(\text{C}_2\text{O}_4)_3]\cdot\text{H}_2\text{O}\}_n$  (**1**) crystalizing in a triclinic space group  $P\bar{1}$ . It was obtained using the building block approach, from the reaction of an aqueous solution of  $[\text{Fe}(\text{C}_2\text{O}_4)_3]^{3-}$  and methanol solutions of  $\text{Cu}^{2+}$  and 2,2'-bipyridine by a layering technique, without the presence of daylight. Structural analysis revealed that this compound contains oxalate-bridged  $[\text{Cu}(\text{bpy})(\mu\text{-C}_2\text{O}_4)\text{Cu}(\text{bpy})]^{2+}$  units linked by oxalate groups of the  $[\text{Fe}(\text{C}_2\text{O}_4)_3]^{3-}$  anions to form the ladder-like 1D  $[\text{Cu}^{\text{II}}\text{Fe}^{\text{III}}]$

chains along the  $a$  axis (Figure 1). Both copper atoms (Cu1 and Cu2) adopt 4 + 2 distorted octahedral coordination; however they are crystallographically and chemically inequivalent: the Cu1 atom is linked to the Fe1 atom by an -O-C-O- bridge, while the Cu2 atom forms bridge to the Fe1 atom only through an O atom of the oxalate molecule. The blue-green crystals of **1** are stable in the matrix in the dark for several months, and when dried from the matrix they can be stored in the refrigerator.<sup>21</sup>

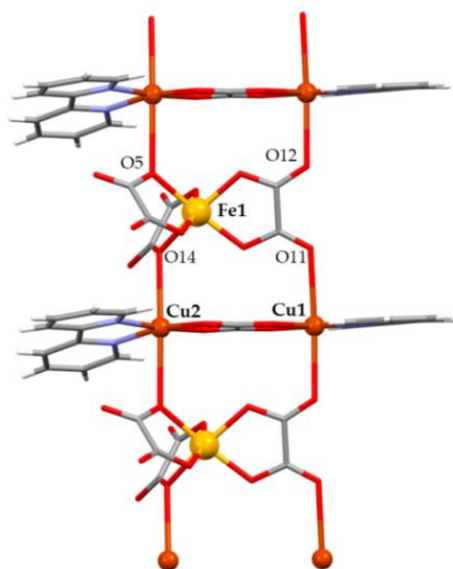


**Figure 1.** The ladder-like 1D chain motif in compound  $\{\text{NH}_4[\{\text{Cu}(\text{bpy})\}_2(\text{C}_2\text{O}_4)\text{Fe}(\text{C}_2\text{O}_4)_3]\cdot\text{H}_2\text{O}\}_n$  (**1**).

The crystals of compound **1** show eye-detectable colour changes when continuously exposed to UV/Vis light in air at room temperature (RT) (Figure 2a). Also, when continuously irradiated with UV/Vis light, the powder sample turns slightly dark in a matter of seconds (referred to below as **1-irrad**) (Figure 2b).

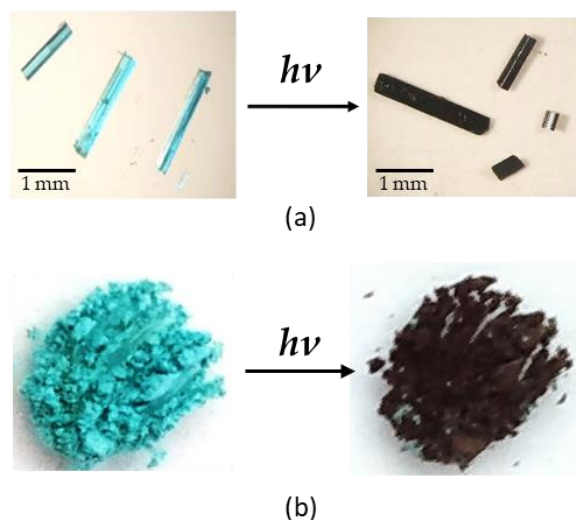


**Figure 2.** The photoinduced colour change of compound **1** (blue-green) to **1-irrad** (dark green) upon continuous irradiation with UV/Vis light of (a) single crystals for 15 minutes; (b) powder sample for 30 minutes.

It is noteworthy that blue-green compound **1** undergoes a photochromic transformation to a dark olive green (hereafter named as **1-irradD**) when exposed to daylight for 18 hours, after which no discernible colour change occurs (Figure 3). It should be noted that while many photochromic coordination polymers are known, those that respond to sunlight/daylight are relatively rare. In general, the use of sunlight for activation may facilitate the practical application of photochromic materials since sunlight is widely available.<sup>28</sup>

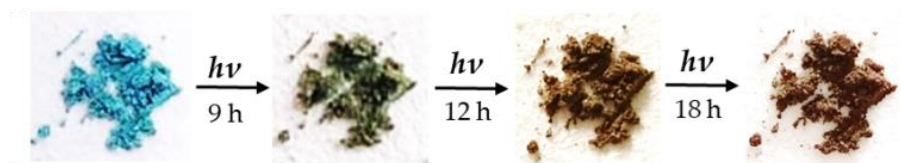


**Figure 3.** Photogenerated colour change of compound **1** after different daylight irradiation times.

The dark green **1-irrad** or **1-irradD** photoproduct is stable in air, and partially returns (visually) to its green colour, hereafter named as **1-recov** or **1-recovD**, after being stored in the dark under an ambient atmosphere for few months (Figure 4). The elevated temperature (70 or 130 °C) has no effect on the colour change of the crystals or powder of **1** in either direction. This slow, reversible transformation indicates that compound **1** has a photoinduced, long-lived, charge-separating state that has been shown to be important for the conversion from solar energy into chemical energy.<sup>28</sup> Many of the reported photochromic materials return to their initial colours within a few minutes.<sup>29</sup>



**Figure 4.** Daylight irradiated compound **1** after being stored in the dark for a different number of days (d).

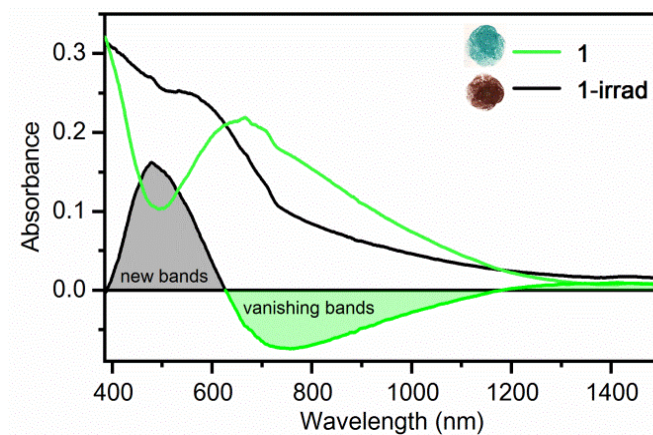
The blue-green crystals of the isostructural compound  $\{K[\{Cu(bpy)\}_2(C_2O_4)Fe(C_2O_4)_3] \cdot H_2O\}_n$  also undergo the same photochromic transformation as compound **1**,<sup>21</sup> whereas, as expected, the crystals of the isostructural compounds containing chromium(III) instead of iron(III),  $\{A[\{Cu(bpy)\}_2(C_2O_4)Cr(C_2O_4)_3] \cdot H_2O\}_n$  ( $A = K^+$  or  $NH_4^+$ ), do not undergo.<sup>30</sup>

**UV/Vis Solid State.** The diffuse reflectance UV/Vis spectra before and after irradiation with UV/Vis light of **1** are shown in Figure 5. Before irradiation, the initial sample **1** (green line, Figure 5) shows overlapped absorption bands in the visible part of the spectrum which are related to: (i)  $d-\sigma_{\text{antibonding}}$  transitions in the tetrahedrally elongated  $[Cu(bpy)(C_2O_4)_2(\mu-C_2O_4)]$

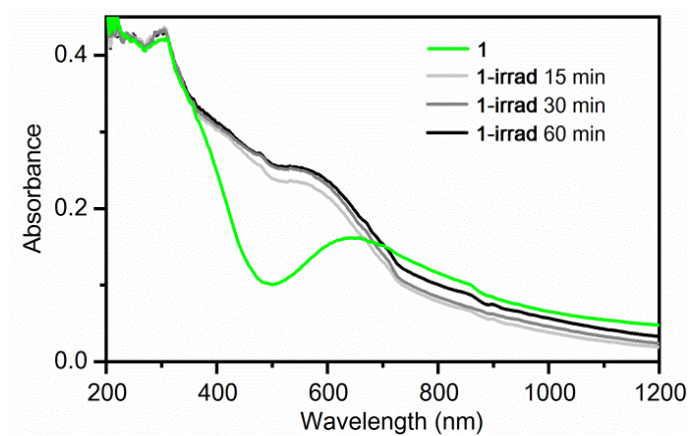
octahedra (bands around 700 nm), and (ii) a charge-transfer transition between the O-donor ligand and high-spin iron(III) atom in octahedral geometry (band around 550 nm).<sup>31</sup>

After irradiation, the absorption intensity in the visible range increase, what is consistent with the blackening of the sample; a new band around 480 nm appears in the spectra, which is related to the ligand-to-metal charge transfer in the  $\text{Fe}^{\text{II}}(\text{C}_2\text{O}_4)_3$  octahedra.<sup>32</sup> Moreover, in the irradiated sample, the bands corresponding to the LMCT transitions of Fe(III) octahedra vanish, and those related to the  $[\text{Cu}(\text{bpy})(\text{C}_2\text{O}_4)_2(\mu\text{-C}_2\text{O}_4)]$  octahedra decrease. This change in the optical properties triggered by UV/Vis light irradiation suggests the reduction of one Fe(III) to Fe(II), and one Cu(II) ion to Cu(I) enabled by the photoinduced oxidation of one oxalate ligand.<sup>18</sup>

When an irradiated compound is left in the dark, some of the Fe(II) ions are being oxidised back to Fe(III) in reaction with  $\text{O}_2$  from the air. This process is very slow, and in the electronic spectra recorded after one month in the dark (1st recovery in Figure 6), the bands associated with Fe(II) ions decrease in intensity at 480 nm, and bands related to Fe(III) ions again appear at 410 and 550 nm. However, the initial spectrum (initial in Figure 6) is not completely recovered, indicating that oxidation occurs only on a fraction of the Fe(II) ions, as a result of the slow kinetics of the oxidation reaction with oxygen from the air at room temperature and pressure. In the following irradiation (2nd irradiation in Figure 6), the intensity of the band at 480 nm increases again, confirming that the recovered Fe(III) ions are again photoreduced to Fe(II). Hence, the colouration and bleaching process of the initial compound can be repeated at least 3 times by UV/Vis irradiation and standing in the dark; the intensity of the green and blackish colour decreases after each cycle.



(a)



(b)

**Figure 5.** (a) Solid-state UV/Vis absorption spectra of **1** (green line) and **1-irrad** (black line), and the difference between the two spectra indicating changes in the electronic properties of **1** due to UV/Vis light irradiation; (b) Evolution of the photogenerated absorption during different irradiation times.

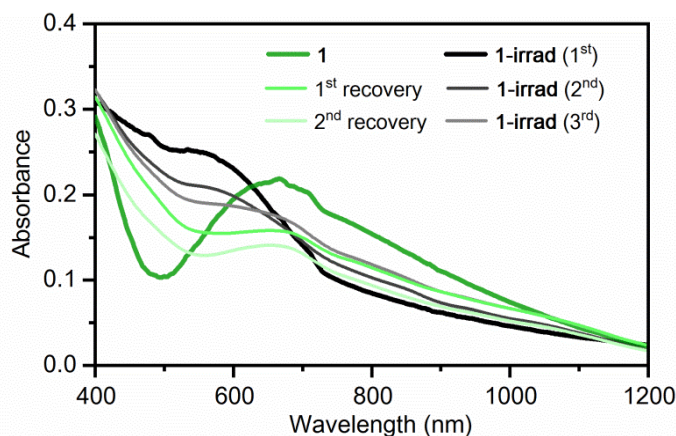


**Figure 6.** Solid-state UV/Vis absorption spectra of compound **1** before (green lines) and after UV/Vis irradiations (black lines). The initial compound underwent three repeated processes of the UV/Vis irradiation and standing in the dark.

**IR Study.** The IR spectra of compound  $\{\text{NH}_4[\{\text{Cu}(\text{bpy})\}_2(\text{C}_2\text{O}_4)\text{Fe}(\text{C}_2\text{O}_4)_3]\cdot\text{H}_2\text{O}\}_n$  pressed in a KBr pellet was recorded before and after irradiation with UV light (Figure 7) at different irradiation times (5 and 45 minutes). Before irradiation, the IR spectrum of **1** exhibits the absorption bands corresponding to the stretching vibrations of the uncoordinated  $\{1709 \text{ and } 1671 \text{ cm}^{-1} [v_{as}(\text{CO})], 1385 \text{ cm}^{-1} [v_s(\text{CO})], 794 \text{ cm}^{-1} [\delta(\text{OCO})]\}$  and coordinated  $\{1645 \text{ cm}^{-1} [v_{as}(\text{CO})], 1356 \text{ cm}^{-1} [v_s(\text{CO})] \text{ and } 781 \text{ cm}^{-1} [\delta(\text{OCO})]\}$  carbonyl of the bidentate-monodentate and bis(bidentate)/bidentate-bis(monodentate) oxalate ligands, respectively.<sup>21</sup> The most striking change in the irradiated sample is the appearance of very strong bands at  $2355, 2341 \text{ and } 666 \text{ cm}^{-1}$  (Figure 7), which originate from the vibrations of carbon dioxide that is being released during the photodecomposition of oxalate and trapped in the KBr pellet during the experiment.<sup>18,33,34</sup> Upon irradiation, the intensity of the bands related to CO stretching vibrations gradually decreases with increasing irradiation time (Figure 7).

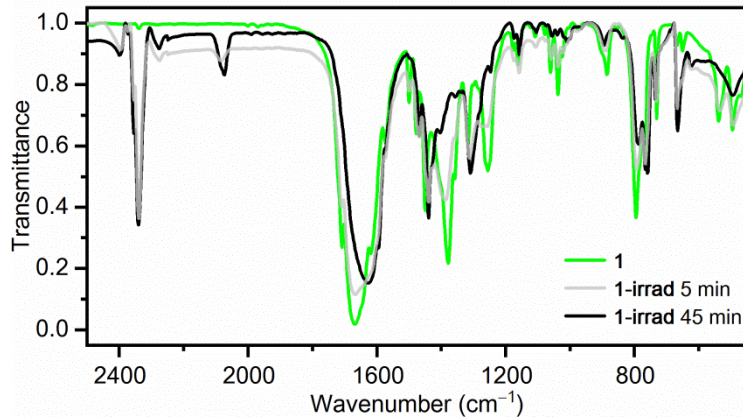


**Figure 7.** Irradiation-time dependence of the IR spectrum for compound **1**. Spectra were recorded at 298 K after 0, 5 and 45 minutes of irradiation with UV light.

These results also confirm a photodecomposition of the oxalate ligands of the tris(oxalato)ferrate(III) unit to the carbon dioxide. As expected, the intense bands of the oxalate groups coordinated to iron and exhibiting bidentate-monodentate mode change more rapidly than other oxalate bands (Figures 1 and 7). The band corresponding to the  $\nu(\text{Fe}^{\text{III}}\text{O})$  located at  $538\text{ cm}^{-1}$  almost disappears after 45 minutes of irradiation; moreover, the intensity of the band at  $494\text{ cm}^{-1}$  [ $\delta(\text{OCO})$ ] decreases,<sup>35</sup> which is also broadened by the appearance of the  $\nu(\text{Fe}^{\text{II}}\text{O})$  band at  $487\text{ cm}^{-1}$ .<sup>36</sup>

**X-ray Diffraction Study.** The single-crystal structure of **1-irrad** could not be determined; several experiments yielded a structure identical to green **1**. The crystals were irradiated so long as they still appeared shiny and crystalline. Close examination of the crystals showed that the darker colour appears only at the surface, to a depth of about  $1\ \mu\text{m}$ . The black **1-irrad** thus forms only on the crystal surface, while its interior remains unchanged. In another experiment, a thin splinter of a crystal several  $\mu\text{m}$  thick was measured before and after irradiation by X-ray diffraction. It is expected that the bulk of this splinter would convert to **1-irrad** upon

irradiation. Despite the small volume of the crystal, the original green splinter (**1**) diffracted rather well, but the darker **1-irrad** diffracted weakly.

The powder X-ray diffraction (PXRD) verified that there was no obvious structural change before (**1**) and after irradiation (**1-irrad**) (Figure 8). This indicates that the photoresponsive behaviour is the result of a chemical charge transfer process rather than a structural transformation. As can be observed in the PXRD, the diffraction lines corresponding to compound **1** are broadened after irradiation. The broadening of the peaks is due to the degradation of the sample as a result of the consumption of the oxalate ligand after irradiation cycle and also because the crystal size decreases during the irradiation process.

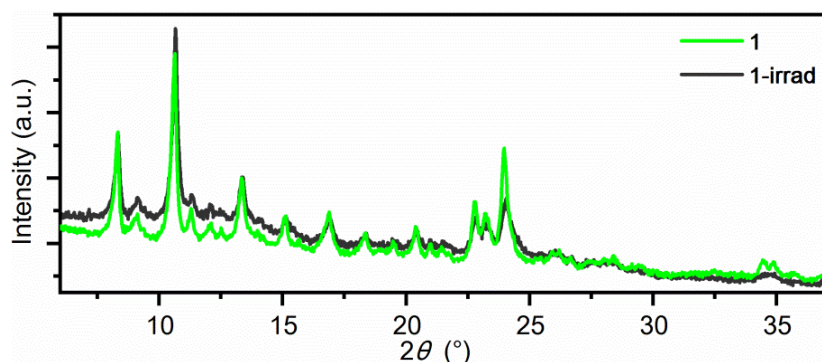


**Figure 8.** Powder XRD patterns of compound  $\{\text{NH}_4[\{\text{Cu}(\text{bpy})\}_2(\text{C}_2\text{O}_4)\text{Fe}(\text{C}_2\text{O}_4)_3]\cdot\text{H}_2\text{O}\}_n$  before (**1**) and after irradiation of 15 min (**1-irrad**).

**Magnetic Study.** The magnetic properties of **1** have already been studied in detail, and from the temperature dependence of the magnetization it was concluded that the two Cu(II) ions with spin 1/2 are antiferromagnetically coupled into the spin singlet within the  $[\text{Cu}(\text{bpy})(\mu\text{-C}_2\text{O}_4)\text{Cu}(\text{bpy})]^{2+}$  units, with relatively large super-exchange interaction across the oxalate bridge. The iron(III) ions have spin 5/2, and do not interact with copper(II) spins.<sup>21</sup> However, at room temperature the  $\chi \cdot T$  product was slightly below the expected value for the independent spins of one iron(III) and two copper(II) ions per

considered formula unit, due to the strong antiferromagnetic exchange between the copper(II) ions of  $-342 \text{ cm}^{-1}$ , which somewhat reduces the overall magnetization.

In this work, the magnetization at room temperature was studied in terms of the field dependence of the molar magnetization  $M_{\text{mol}}(H)$  for both **1** and **1-irrad**, the measurements of which are shown in Figure 9. From the  $M_{\text{mol}}(H)$  dependence for **1** at 300 K (dark green symbols), the slope is  $(1.584 \pm 0.001) \cdot 10^{-2} \text{ emu} \cdot \text{mol}^{-1} \cdot \text{Oe}^{-1}$ , and after multiplication by the temperature 300 K, the product  $\chi \cdot T$  is obtained to be  $(4.752 \pm 0.003) \text{ emu} \cdot \text{K} \cdot \text{mol}^{-1} \cdot \text{Oe}^{-1}$ . For completely independent spins, this product should be  $5.24 \text{ emu} \cdot \text{K} \cdot \text{mol}^{-1} \cdot \text{Oe}^{-1}$  for one Fe(III) ion with spin 5/2 and two Cu(II) ions with spin 1/2, and the observed difference is comparable to the difference between the susceptibility of an antiferromagnetic dimer with super-exchange interaction of order 200–300 K and the susceptibility of two free copper(II) ions, which is in full agreement with previous study.<sup>21</sup> For all calculations the usual values of  $g$ -factors from the literature were used: 2.15 for copper and 2.0 for iron.<sup>37</sup> After irradiation, the sample was measured again in the magnetometer, and the  $M_{\text{mol}}(H)$  dependence for **1-irrad** at 300 K (black symbols) significantly decreased compared with **1**. From the slope  $(1.126 \pm 0.005) \cdot 10^{-2} \text{ emu} \cdot \text{mol}^{-1} \cdot \text{Oe}^{-1}$  multiplied by 300 K, the  $\chi \cdot T$  product is  $(3.38 \pm 0.01) \text{ emu} \cdot \text{K} \cdot \text{mol}^{-1} \cdot \text{Oe}^{-1}$ . This value corresponds to one copper(II) ion with spin 1/2 and an iron(II) ion with spin 2, which would ideally give  $3.435 \cdot 10^{-2} \text{ emu} \cdot \text{mol}^{-1} \cdot \text{Oe}^{-1}$ , and this small difference could be ascribed to slightly different  $g$ -factors.

Therefore, the observed decrease in molar magnetization can be ascribed with high probability to the reduction of  $[\text{Cu}^{\text{II}}(\text{bpy})(\mu\text{-C}_2\text{O}_4)\text{Cu}^{\text{II}}(\text{bpy})]^{2+}$  to  $[\text{Cu}^{\text{I}}(\text{bpy})(\mu\text{-$

$\text{C}_2\text{O}_4\text{Cu}^{\text{II}}(\text{bpy})^{\text{I}}]^+$  units, and Fe(III) to Fe(II) ions. The values indicate that these changes occur in the vast majority of the sample, which is accomplished due to the finely powdered microcrystals.

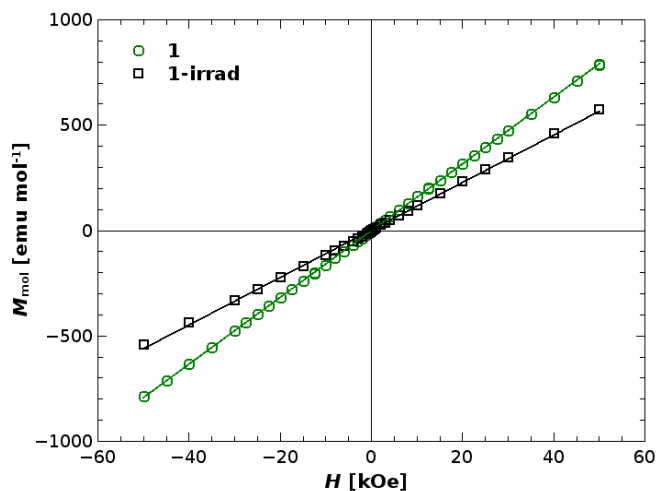


**Figure 9.** Field dependence of the molar magnetization of compound **1** measured at room temperature (300 K) before (dark green symbols and line) and after (black symbols and line) irradiation.

**EPR Study.** The light-induced colouration of **1** is accompanied also by an EPR study. Figure 10 shows the spectra of samples **1** and **1-irrad** (2 hours of irradiation) recorded at room (RT) and at low (LT, 80 K) temperature. The RT spectrum of **1** (Figure 10a) shows a signal from paramagnetic Fe(III) ions labelled by  $g \approx 4.8$  (at line maximum position)<sup>38</sup> and one broad line around  $g \approx 2.1$  that could be assigned to Cu(II) ions coupled through the oxalate bridge.<sup>39</sup> Besides these two lines, an additional line typical for paramagnetic (non-coupled) Cu(II), labelled by  $g \approx 2.07$ , could be seen.<sup>40</sup> After 2 hours of UV irradiation, Fe(III) line almost completely disappears. Additionally, the broad copper line around  $g \approx 2.1$  also disappears.

The irradiation-induced change in the EPR lines is more evident in the LT spectra, shown in Figure 10b, where the broad copper line is not observed due to stronger

antiferromagnetic coupling between copper spins from the  $[\text{Cu}(\text{bpy})(\mu\text{-C}_2\text{O}_4)\text{Cu}(\text{bpy})]^{2+}$  units (see Magnetic study). As can be seen, the intensity of Fe(III) line decreases after irradiation. It should be stressed here that the mass of **1-irrad** sample was a few times smaller compared to the mass of the pristine sample **1**, so a direct comparison of line intensities before and after the irradiation process is not possible. Moreover, samples with different masses were used for the measurements at RT and LT, so a direct comparison of the intensities of the spectral lines at RT and LT is not possible. The reason why the Fe(III) line did not completely disappear at LT and did at RT is probably due to the larger mass of the sample used at LT (we tried to keep the irradiation time the same). Therefore a longer irradiation time should be performed to observe the complete disappearance of the Fe(III) line. Additionally, it should be noted here, that Fe(II) ions are usually X-band EPR silent but their presence can be proved by bulk magnetization measurements or high-frequency EPR spectroscopy.

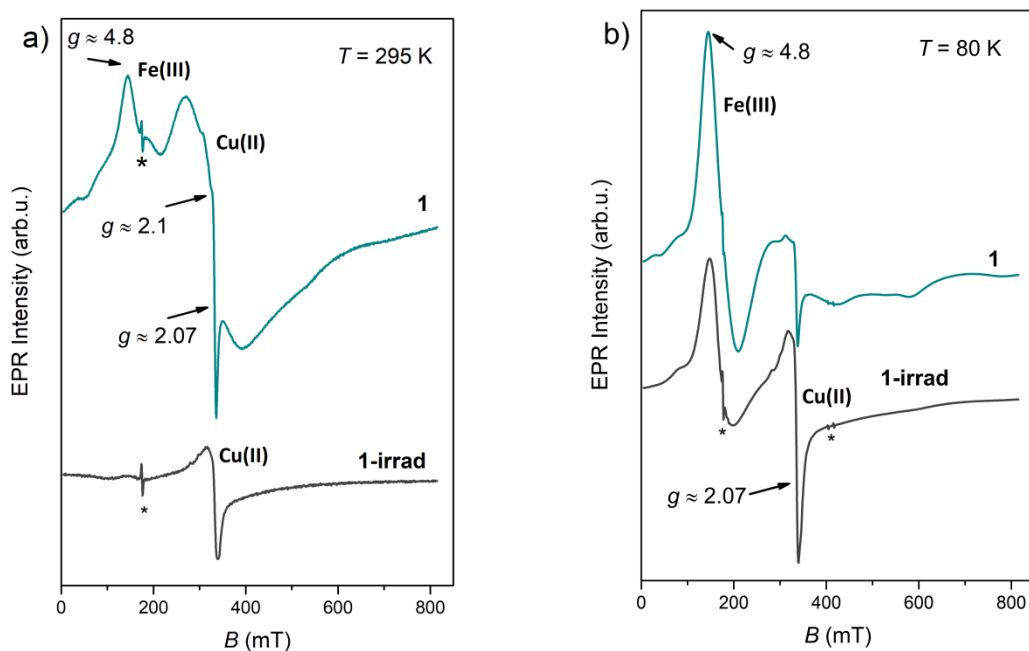


**Figure 10.** The EPR spectra of **1** and **1-irrad** recorded at (a) room temperature and (b) 80 K. Sharp lines labelled by asterisks are EPR cavity signal.

**Electrical Study.** The electrical conductivity of compound **1** before and after irradiation was measured by impedance spectroscopy. The complex impedance plot of **1** at 20 °C shows an arc at high values of impedance revealing very low electrical conductivity, whereas **1-irrad** exhibits a well-defined depressed semicircle at significantly lower values of impedance (see Figure 11). The obtained experimental impedance spectra can be well approximated by the equivalent circuit consisting of a parallel combination of resistor and constant phase element (CPE). The CPE is an empirical impedance function of the type  $Z^*_{CPE} = 1/[A(i\omega)^\alpha]$ , where  $\omega = 2\pi f$ ,  $f$  is the measuring frequency,  $i = (-1)^{1/2}$  is the imaginary unit,  $A$  is the constant, and  $\alpha$  is a power law exponent with a value in the range of  $0 < \alpha < 1$ . For  $\alpha = 1$ , the CPE acts as an ideal capacitor, whereas for  $\alpha = 0$ , it is a resistor. The values of electrical resistance ( $R$ ) at 20 °C of **1** and **1-irrad** obtained by the complex non-linear least squares fitting are given in the legends in Figure 11. From the value of electrical resistance ( $R$ ) and electrode dimensions (where  $d$  is the thickness of the sample and  $A$  is the electrode area), DC conductivity,  $\sigma_{DC}$ , was calculated using the relation:  $\sigma_{DC} = d/(A \cdot R)$ . The electrical conductivity of **1** at 20 °C is very low,  $\sigma_{DC} = 8.8 \times 10^{-16} (\Omega \text{ cm})^{-1}$ , however it increases approximately four orders of magnitude upon irradiation [ $\sigma_{DC} = 3.8 \times 10^{-12} (\Omega \text{ cm})^{-1}$ ]. The observed increase in conductivity is in line with the structural and magnetic properties described in the previous sections, and can be related to the mixed oxidation states of iron and copper in an irradiated sample, which allow electron transfer to occur, hence increasing electrical conductivity. Similar examples of the electronic transport were reported for many mixed-valence coordination polymers, in particular for those containing  $\text{Cu(I)Cu(II)}$ <sup>41,42</sup> and  $\text{Fe(II)Fe(III)}$ .<sup>41-43</sup>

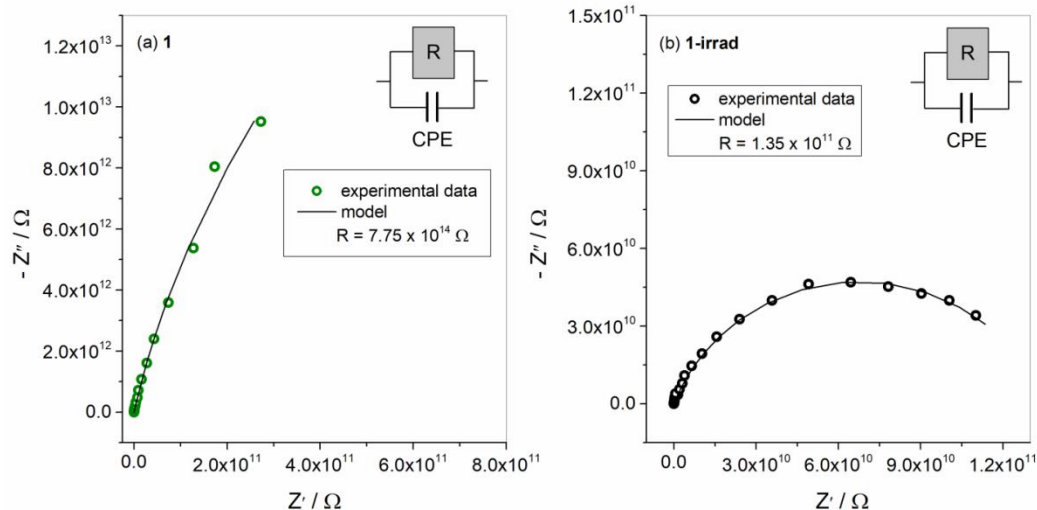


**Figure 11.** Complex impedance plots measured at 20 °C for (a) **1** and (b) **1-irrad** and their corresponding equivalent circuits.

**DFT Calculations.** The electronic structure of compound **1** was calculated using DFT to confirm the possibility of the proposed light-induced intramolecular electron transfers. In agreement with other experiments, the obtained ground state consists of antiferromagnetically coupled Cu(II) ions and paramagnetic Fe(III) ions. Figure 12 shows the density of states projected on atomic orbitals per atomic type. Oxygen has the largest contribution to the top of the valence band, while the bottom of the conduction band is mostly made of Cu and Fe orbitals *d*. Thus, it is expected that upon irradiation electrons from the top of the valence band would fill the bottom of the conduction band, i.e., the Cu and Fe orbitals *d*, which would explain the electron transfers from the oxalate ligand to Fe(III) and to Cu(II) and the change to Cu(I) and Fe(II).

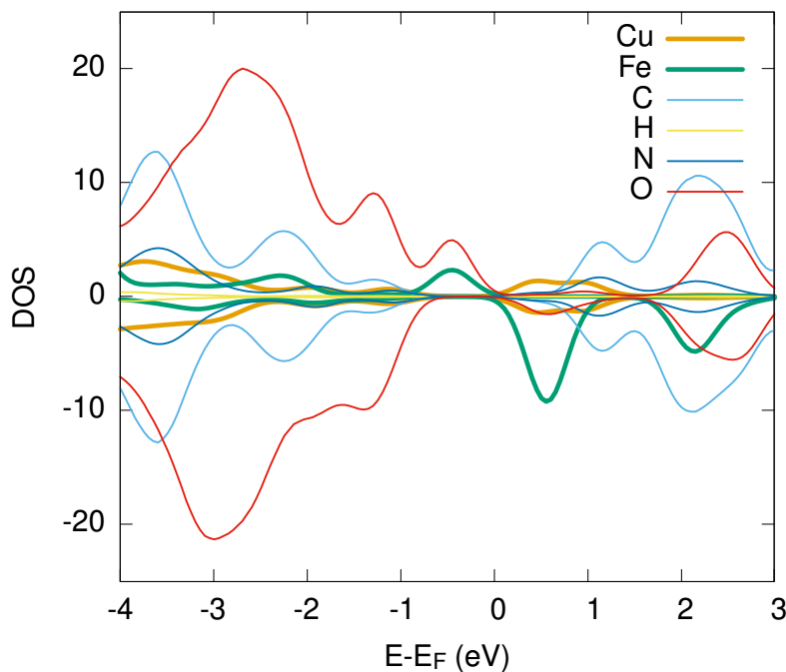


**Figure 12.** Projected electronic density of states of compound **1** obtained by DFT.

## CONCLUSIONS

Compound **1** was investigated for its photosensitive properties, as it exhibits an intense coloration (from blue-green to black/dark green) in the solid state when irradiated with UV/Vis light or daylight. The effect is related to ligand-to-metal charge transfer, from the oxalate ligand to Fe(III) ions due to the partial photodecomposition of the oxalate ligand (photodissociation of the coordinated bond between Fe(III) and the oxygen atom) and reduction to Fe(II), together with the formation of a carbon dioxide radical ion ( $\text{CO}_2^{\cdot-}$ ). Simultaneously, the radical ion most likely reacts with the cationic units  $[\{\text{Cu}(\text{bpy})\}_2(\mu\text{-C}_2\text{O}_4)]^{2+}$  forming reduced, diamagnetic Cu(I) ion and gaseous  $\text{CO}_2$  is released. The other copper atom of the oxalate-bridged cationic moiety remains in the +2 oxidation state, as confirmed by magnetic research, implying that during the photocoloration process two electrons are released from the oxalate ligand and accepted by the metal atoms, followed by decomposition of the reactive oxalate.<sup>18</sup> This photochromic mechanism

and the property changes caused by the irradiation were investigated, confirmed and explained by complementing different techniques and methods of characterization in the solid state before and after the irradiation of compound **1**: powder X-ray diffraction, diffuse reflectance UV/Vis, IR and EPR spectroscopy, magnetization and impedance measurements, and DFT calculations.

As functional molecular materials with stimulative and switchable properties are attracting interest from fundamental research to future applications, our further investigation would aim at the synthesis and characterization of novel complexes with the  $[\text{Fe}(\text{C}_2\text{O}_4)_3]^{3-}$  core, leading to various photosensitive systems with tuneable properties based on electron transfer, as those of optical, magnetic and electrical in coordination polymer **1**.

## **ASSOCIATED CONTENT**

### **Funding**

This work has been funded and supported by the Croatian Science Foundation Project No. IP-2019-04-5742.

### **Notes**

The authors declare no competing financial interest.

### **Acknowledgement**

D. B. and D. P. acknowledge the support of project CeNIKS cofinanced by the Croatian Government and the European Union through the European Regional Development Fund – Competitiveness and Cohesion Operational Programme (Grant KK.01.1.1.02.0013). D. Ž. thanks HrZZ IP-2018-01-3168 project for financial support.

## **AUTHOR INFORMATION**

### **Corresponding Author**

**\*Dr. Marijana Jurić**

Ruđer Bošković Institute

Bijenička cesta 54

10000 Zagreb, Croatia

Phone: +385 1 4561189. Fax: +385 1 4680098.

E-mail: Marijana.Juric@irb.hr. (M.J.)

## REFERENCES

- (1) Ru, Y.; Shi, Z.; Zhang, J.; Wang, J.; Chen, B.; Huang, R.; Liu, G.; Yu, T. Recent progress of photochromic materials towards photocontrollable devices. *Mater. Chem. Front.* **2021**, *5*, 7737–7758.
- (2) Rice, A. M.; Martin, C. R.; Galitskiy, V. A.; Berseneva, A. A.; Leith, G. A.; Shustova, N. B. Photophysics Modulation in Photoswitchable Metal–Organic Frameworks. *Chem. Rev.* **2020**, *120*, 8790–8813.
- (3) Zhang, J.; Zou, Q.; Tian, H. Photochromic Materials: More Than Meets The Eye, *Adv. Mater.* **2013**, *25*, 378–399.
- (4) Xiang, F.; Chen, S.; Yuan, Z.; Li, L.; Fan, Z.; Yao, Z.; Liu, C.; Xiang, S.; Zhang, Z. Switched Proton Conduction in Metal–Organic Frameworks. *JACS Au* **2022**, *2*, 1043–1053.
- (5) Dunatov, M.; Puškarić, A.; Pavić, L.; Štefanić, Z.; Androš Dubraja, L. Electrically responsive structural transformations triggered by vapour and temperature in a series of pleochroic bis(oxalato)chromium(III) complex salts. *J. Mater. Chem. C* **2022**, *10*, 8024–8033.
- (6) Li, H.-Y.; Xu, H.; Zang, S.-Q.; Mak, T. C. W. A viologen-functionalized chiral Eu-MOF as a platform for multifunctional switchable material. *Chem. Commun.* **2016**, *52*, 525–528.

- (7) Han, S.-D.; Hu J.-X.; Wang, G.-M. Recent advances in crystalline hybrid photochromic materials driven by electron transfer. *Coord. Chem. Rev.* **2022**, *452*, 214304.
- (8) Pardo, R.; Zayat, M.; Levy, D. Photochromic organic–inorganic hybrid materials. *Chem. Soc. Rev.* **2011**, *40*, 672–687.
- (9) Dunatov, M.; Puškarić, A.; Androš Dubraja, L. Multi-stimuli responsive (l-tartrato)oxovanadium(v) complex salt with ferroelectric switching and thermistor properties. *J. Mater. Chem. C* **2023**, *11*, 2880–2888.
- (10) Mehlana, G.; Bourne, S. A. Unravelling chromism in metal–organic frameworks. *CrystEngComm* **2017**, *19*, 4238–4259.
- (11) Lustig, W. P.; Mukherjee, S.; Rudd, N. D.; Desai, A. V.; Li, J.; Ghosh, S. K. Metal–organic frameworks: functional luminescent and photonic materials for sensing applications. *Chem. Soc. Rev.* **2017**, *46*, 3242–3285.
- (12) Halder, R.; Heinke, L.; Wöll, C. Advanced Photoresponsive Materials Using the Metal–Organic Framework Approach. *Adv. Mater.* **2020**, *32*, 1905227.
- (13) Shen, J.-J.; Wang, F.; Yu, T.-L.; Zhang, F.-Q.; Tian, L.; Fu, Y.-L. Halogen-dependent photoinduced electron transfer and chromism of three protonated nicotinohydrazide halozincates. *Dalton Trans.* **2017**, *46*, 5414–5419.
- (14) Rice, A. M.; Martin, C. R.; Galitskiy, V. A.; Berseneva, A. A.; Leith, G. A.; Shustova, N. B. Photophysics Modulation in Photoswitchable Metal–Organic Frameworks. *Chem. Rev.* **2020**, *120*, 8790–8813.

- (15) Deguillaume, L.; Leriche, M.; Desboeufs, K.; Mailhot, G.; George, C.; Chaumerliac, N. Transition Metals in Atmospheric Liquid Phases: Sources, Reactivity, and Sensitive Parameters. *Chem. Rev.* **2005**, *105*, 3388–3431.
- (16) Mangiante, D. M.; Schaller, R. D.; Zarzycki, P.; Banfield, J. F.; Gilbert, B. Mechanism of Ferric Oxalate Photolysis. *ACS Earth Space Chem.* **2017**, *1*, 270–276.
- (17) Ogi, Y.; Obara, Y.; Katayama, T.; Suzuki, Y.-I.; Liu, S. Y.; Bartlett, N. C.-M.; Kurahashi, N.; Karashima, S.; Togashi, T.; Inubushi, Y.; Ogawa, K.; Owada, S.; Rubešová, M.; Yabashi, M.; Misawa, K.; Slaviček, P.; Suzuki, T. Ultraviolet photochemical reaction of  $[\text{Fe(III)}(\text{C}_2\text{O}_4)_3]^{3-}$  in aqueous solutions studied by femtosecond time-resolved X-ray absorption spectroscopy using an X-ray free electron laser. *Struct. Dyn.* **2015**, *2*, 034901.
- (18) Duan, Y.; Waerenborgh, J. C.; Clemente-Juan, J. M.; Giménez-Saiz, C.; Coronado, E. Light-induced decarboxylation in a photo-responsive iron-containing complex based on polyoxometalate and oxalato ligands. *Chem. Sci.* **2017**, *8*, 305–315.
- (19) Muzioł, T. M.; Tereba, N.; Podgajny, R.; Kędziera D.; Wrzeszcz, G. Solvent-assisted structural conversion involving bimetallic complexes based on the tris(oxalato) ferrate(III) unit with the green → blue → red crystal color sequence. *Dalton Trans.* **2019**, *48*, 11536–11546.
- (20) Rabani, J.; Mamane, H.; Pousty, D.; Bolton, J. R. Practical Chemical Actinometry—A Review. *Photochem. Photobiol.* **2021**, *97*, 873–902.
- (21) Kanižaj, L.; Androš Dubraja, L.; Torić, F.; Pajić, D.; Molčanov, K.; Wenger, E.; Jurić, M. Dimensionality controlled by light exposure: 1D versus 3D oxalate-bridged [CuFe] coordination polymers based on an  $[\text{Fe}(\text{C}_2\text{O}_4)_3]^{3-}$  metallotecton. *Inorg. Chem. Front.* **2019**, *6*, 3327–3335.

(22) Inorganic Syntheses. ed. H. S. Booth, McGraw-Hill Book Company, INC., New York and London, 1939.

(23) Giannozzi, P.; Andreussi, O.; Brumme, T.; Bunau, O.; Buongiorno Nardelli, M.; Calandra, M.; Car, R.; Cavazzoni, C.; Ceresoli, D.; Cococcioni, M.; Colonna, N.; Carnimeo, I.; Dal Corso, A.; de Gironcoli, S.; Delugas, P.; DiStasio Jr, R. A.; Ferretti, A.; Floris, A.; Fratesi, G.; Fugallo, G.; Gebauer, R.; Gerstmann, U.; Giustino, F.; Gorni, T.; Jia, J.; Kawamura, M.; Ko, H.-Y.; Kokalj, A.; Küçükbenli, E.; Lazzeri, M.; Marsili, M.; Marzari, N.; Mauri, F.; Nguyen, N. L.; Nguyen, H.-V.; Otero-de-la-Roza, A.; Paulatto, L.; Poncé, S.; Rocca, D.; Sabatini, R.; Santra, B.; Schlipf, M.; Seitsonen, A. P.; Smogunov, A.; Timrov, I.; Thonhauser, T.; Umari, P.; Vast, N.; Wu, X.; Baroni, S. Advanced capabilities for materials modelling with Quantum ESPRESSO, *J. Phys.: Condens. Matter* 2017, **29**, 465901.

(24) Giannozzi, P.; Baroni, S.; Bonini, N.; Calandra, M.; Car, R.; Cavazzoni, C.; Ceresoli, D.; Chiarotti, G. L.; Cococcioni, M.; Dabo, I.; Dal Corso, A.; de Gironcoli, S.; Fabris, S.; Fratesi, G.; Gebauer, R.; Gerstmann, U.; Gougoussis, C.; Kokalj, A.; Lazzeri, M.; Martin-Samos, L.; Marzari, N.; Mauri, F.; Mazzarello, R.; Paolini, S.; Pasquarello, A.; Paulatto, L.; Sbraccia, C.; Scandolo, S.; Sclauzero, G.; Seitsonen, A. P.; Smogunov, A.; Umari, P.; Wentzcovitch, R. M. QUANTUM ESPRESSO: a modular and open-source software project for quantum simulations of materials. *J. Phys.: Condens. Matter* **2009**, *21*, 395502.

(25) Prandini, G.; Marrazzo, A.; Castelli, I. E.; Mounet, N.; Marzari, N. Precision and efficiency in solid-state pseudopotential calculations. *npj Comput. Mater.* **2018**, *4*, 72.

(26) Perdew, J. P.; Burkeand, K.; Ernzerhof, M. Generalized Gradient Approximation Made Simple. *Phys. Rev. Lett.* **1997**, *78*, 1396.

- (27) Dudarev, S. L.; Botton, G. A.; Savrasov, S. Y.; Humphreys, C. J.; Sutton, A. P. Electron-energy-loss spectra and the structural stability of nickel oxide: An LSDA+U study. *Phys. Rev. B* **1998**, *57*, 1505.
- (28) Kan, W.-Q.; Wen, S.-Z.; He, Y.-C.; Xu, C.-Y. Viologen-Based Photochromic Coordination Polymers for Inkless and Erasable Prints. *Inorg. Chem.* **2017**, *56*, 14926–14935.
- (29) Li, P.-X.; Wang, M.-S.; Guo, G.-C. Two new coordination compounds with a photoactive pyridinium-based inner salt: influence of coordination on photochromism. *Cryst. Growth Des.* **2016**, *16*, 3709–3715.
- (30) Kanižaj, L.; Molčanov, K.; Torić, F.; Pajić, D.; Lončarić, I.; Šantić, A.; Jurić, M. Ladder-like [CrCu] coordination polymers containing unique bridging modes of  $[\text{Cr}(\text{C}_2\text{O}_4)_3]^{3-}$  and  $\text{Cr}_2\text{O}_7^{2-}$ . *Dalton Trans.* **2019**, *48*, 7891–7898.
- (31) Solomon, E. I.; Lever, A. B. P. *Inorganic Electronic Structure and Spectroscopy*, John Wiley & Sons, Inc., Hoboken, New Jersey, 2006.
- (32) Cococcioni, M.; de Gironcoli, S. Linear response approach to the calculation of the effective interaction parameters in the LDA+U method, *Phys. Rev. B* **2005**, *71*, 035105.
- (33) Gerakines, P. A. Schutte, W. A. Greenberg J. M.; van Dishoeck, E. F. The infrared band strengths of H<sub>2</sub>O, CO and CO<sub>2</sub> in laboratory simulations of astrophysical ice mixtures. *Astron. Astrophys.* **1995**, *296*, 810–818.
- (34) Zhang, X.; Sander, S. P. Infrared Absorption Spectra of the CO<sub>2</sub>/H<sub>2</sub>O Complex in a Cryogenic Nitrogen Matrix—Detection of a New Bending Frequency, *J. Phys. Chem. A* **2011**, *115*, 9854–9860.

- (35) Nakamoto, K. *Infrared and Raman Spectra of Inorganic and Coordination Compounds*. 6th ed., John Wiley, New York, 2009.
- (36) Pegu, R.; Majumdar, K. J.; Talukdar, D. J.; Pratihar, S. Oxalate capped iron nanomaterial: from methylene blue degradation to bis(indolyl)methane synthesis. *RSC Adv.* **2014**, *4*, 33446–33456.
- (37) Kahn, O. *Molecular Magnetism*. Wiley-VCH: New York, 1993.
- (38) Bou-Abdallah, F.; Chasteen, N. D. Spin concentration measurements of high-spin ( $g' = 4.3$ ) rhombic iron(III) ions in biological samples: theory and application. *J. Biol. Inorg. Chem.* **2008**, *13*, 15–24.
- (39) Bencini, A.; Gatteschi, D. *Electron paramagnetic resonance of exchange coupled systems*. Springer, Berlin, 1990.
- (40) Garribba, E.; Micera, G. The Determination of the Geometry of Cu(II) Complexes: An EPR Spectroscopy Experiment. *J. Chem. Educ.* **2006**, *83*, 1229–1232.
- (41) Murase, R.; Leong, C. F.; D'Alessandro, D. M. Mixed Valency as a Strategy for Achieving Charge Delocalization in Semiconducting and Conducting Framework Materials. *Inorg. Chem.* **2017**, *56*, 14373–14382.
- (42) Givaja, G.; Amo-Ochoa, P.; J. Gómez-García, C. J.; Zamora, F. Electrical conductive coordination polymers. *Chem. Soc. Rev.* **2012**, *41*, 115–147.
- (43) Sahadevan, S. A.; Abhervé, A.; Monni, N.; de Pipaón, C. S.; Galán-Mascarós, J. R.; Waerenborgh, J. C.; Vieira, B. J. C.; Auban-Senzier, P.; Pillet, S.; Bendeif, El-E.; Alemany, P.; Canadell, E.; Mercuri, M. L., Avarvari, N. Conducting Anilate-Based Mixed-Valence

Fe(II)Fe(III) Coordination Polymer: Small-Polaron Hopping Model for Oxalate-Type Fe(II)Fe(III) 2D Networks. *J. Am. Chem. Soc.* **2018**, *140*, 12611–12621.

## TABLE OF CONTENTS SYNOPSIS

1D ladder-like heterometallic compound obtained using  $[\text{Fe}(\text{C}_2\text{O}_4)_3]^{3-}$ , exhibits a photocoloration effect when exposed to direct sunlight or UV/Vis irradiation, which involves a simultaneous intramolecular electron transfers from the oxalate ligand confirmed by various techniques.

